RPE Radiation Physics & Engineering
A Peer-Reviewed Journal
Published by K.N. Toosi University of Technology
http://rpe.kntu.ac.ir
Research Article

Radiation Physics and Engineering 2023; 4(4):43–50

Two-dimensional simulation of argon dielectric barrier discharge (DBD) plasma actuator with COMSOL Multiphysics

Ramin Mehrabifard*

Department of Physics and Institute for Plasma Research, Kharazmi University, 49 Dr. Mofatteh Avenue, Tehran, Iran

HIGHLIGHTS

- Investigating the two-dimensional discharge behavior of Argon gas in the plasma actuator structure.
- Investigating the effect of the distance of the electrode buried in the dielectric on parameters affecting the body force.
- The effect of dielectric material on the key parameters of plasma actuator had been analyzed.

ABSTRACT

Dielectric barrier discharge (DBD) plasma is used for various applications. DBD is also one of the most efficient and low-cost methods for active fluid flow control. In this study, a detailed physical model of DBD in atmospheric pressure at 1 kV DC voltage is developed with COMSOL Multiphysics software. Argon gas is also used as a background gas and electrodes are assumed to be copper. Plasma parameters such as electron and ion density, electric field, potential, and temperature for different gap distances of electrodes (1.0 mm, 0.9 mm, 0.8 mm) and different dielectric type (Quartz, Silica Glass, Mica). The results of the simulation show that the longitudinal distance of the grounded electrodes to the power electrodes has a direct influence on parameters such as electron temperature, and electron and ion density which are the main factors of fluid flow control. These parameters have the maximum value when Mica is used as a dielectric and the lowest value when Silica Glass is utilized.

KEYWORDS

Dielectric Barrier Discharge
Argon Plasma
Plasma Actuator
Body Force
COMSOL Multiphysics
Gas Discharge

HISTORY

Received: 6 April 2023
Revised: 29 May 2023
Accepted: 14 June 2023
Published: Autumn 2023

1 Introduction

Due to its exceptional features, cold atmospheric pressure plasma (CAP) has been applied in a wide range of scientific fields (Da Ponte et al., 2012; Hati et al., 2012; Lukes et al., 2014; Mehrabifard et al., 2020; Zimmermann et al., 2011). CAPs can involve partially ionized gas, many active species (positive/negative ions, radicals), UV radiation, and transient electric field (Graves, 2012; Mehrabifard et al., 2017; Weltmann et al., 2010). In the context of plasma actuators, a body force refers to the force exerted on a fluid (such as air) by the plasma discharge. Plasma actuators are devices that use plasma discharges to generate localized airflow control, typically in aerospace and fluid dynamics applications. Controlling the separation of flow with the use of atmospheric pressure cold plasma is considered very promising (Jayaraman et al., 2007; Shang and Huang, 2014; Sohbatzadeh et al., 2019). The separation of the flow from the surface will occur at high angles of attack, angle between the chord line of the flying object and the direction of the oncoming airflow, in a variety of cases, including diffusers, cars, feathers of turbines and airfoils, and will always be accompanied by losses, which will significantly reduce the performance parameters and efficiency. The cold plasma can control this flow by making the body force produced by the difference in charge particle and the electric field in the system (Boeuf et al., 2007). Several methods are used to obtain the body force created by the non-equilibrium plasma (Abdollahzadeh et al., 2012).

Different models of atmospheric pressure discharge are also used to create body force including direct discharge, microwave discharge, corona discharge, spark and dielectric barrier discharge (Boeuf et al., 2007; Georghiou et al., 2005; Shang and Huang, 2010). Therefore, the dielectric barrier discharge is one of the most common methods for

*Corresponding author: std_r.mehrabifard@alumni.khu.ac.ir

https://doi.org/10.22034/rpe.2023.392080.1127

https://dorl.net/dor/20.1001.1.26456397.2023.4.4.6.6

Table 1: Table of collisions and reactions modeled.

Reactions	Formula	Type	$\Delta\varepsilon$ (eV)
1	e + Ar → e + Ar	Elastic	0
2	e + Ar → e + Ars	Excitation	11.5
3	e + Ars → e + Ar	Super-elastic	-11.5
4	e + Ar → 2e + Ar^+	Ionization	15.8
5	e + Ars → 2e + Ar^+	Ionization	4.24
6	Ars + Ars → e + Ar + Ar^+	Penning ionization	-
7	Ars + Ar → Ar + Ar	Metastable quenching	-

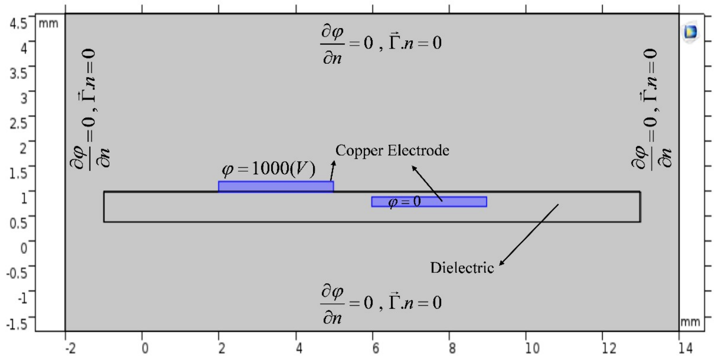

Figure 1: Plasma actuator structure and boundary condition in surrounding space.

creating body force (Lieberman and Lichtenberg, 1994). In the plasma actuator, the structure of the electrodes is non-symmetrical that are located two sides of the dielectric. Many researchers have used numerical codes to simulate plasma. Studies have shown that in previous work, due to the use of numerical codes, the number of reactions considered for discharge and surface reactions are limited (Soloviev and Krivtsov, 2009).

In this research, all the characteristics of an electric discharge of argon gas in a two-dimensional structure used in a plasma actuator have been evaluated. And the effect of the gap distances of the electrodes from each other and the dielectric material type, on the body force main parameters (net charge and electric field magnitude) has been investigated.

2 Plasma model

2.1 Geometry and Description

The general schematic of the actuator is shown in Fig. 1. Copper electrodes dimensions are 0.2 mm×0.3 mm and the dielectric dimensions are 0.6 mm×14 mm. The gas used in this structure is argon, which contains neutral particles, electrons, negative ions, and positive ions. The total space around the structure involves argon. The input voltage leads to the production or consumption of each component. Argon reacts in different forms on the surface as the most probable reactions are the seven ones shown in Table 1.

In most of the studies that have been done in this field, a reaction has been used to simplify the calculations. Increasing reactions also result in longer computing time. In addition to the seven reactions mentioned above, two surface reactions are considered, as shown in Table 2. For meshing this structure, we use 5 boundary layers and 1.4 stretching factor for whole boundary of system. For entire geometry a free triangular mesh is used with maximum element size of 0.4 (see Fig. 2).

Table 2: Table of surface reactions.

Reaction	Formula	Sticking Coefficient
1	Ars → Ar	1
2	Ar^+ → Ar	1

In this study, the fluid model was used. By solving the drift-diffusion equations, the electron density and energy will be obtained. The governing equations for electric discharge with the drift-diffusion approximation are as follows:

$$\frac{\partial n_e}{\partial t} + \nabla.\vec{\Gamma}_e = R_e - (\vec{u}.\nabla)n_e \tag{1}$$

$$\vec{\Gamma}_e = -(\vec{\Gamma}_e.\vec{E}) - \vec{D}_e.\nabla n_e \tag{2}$$

Equation (1) defined the electron continuity equation. In Eq. (1), n_e is the electron density, D_e is electron diffusion coefficient, Γ_e represents electron flux, u is average velocity of the species and R_e is the electron production rate. Equation (2) is electron flux, which consists of two parts: drift and diffusion. The electron energy density is calculated by the following equation:

$$\begin{aligned} &\frac{\partial n_\varepsilon}{\partial t} + \nabla.\vec{\Gamma}_\varepsilon + \vec{E}.\vec{\Gamma}_\varepsilon = R_\varepsilon - (\vec{u}.\nabla)n_e \\ &\vec{\Gamma}_\varepsilon = -(\vec{\Gamma}_\varepsilon.\vec{E}) - \vec{D}_\varepsilon.\nabla n_\varepsilon \end{aligned} \tag{3}$$

This expression $\vec{E}.\vec{\Gamma}_\varepsilon$ represents the amount of energy obtained form an electron by electric field. R_e is the energy

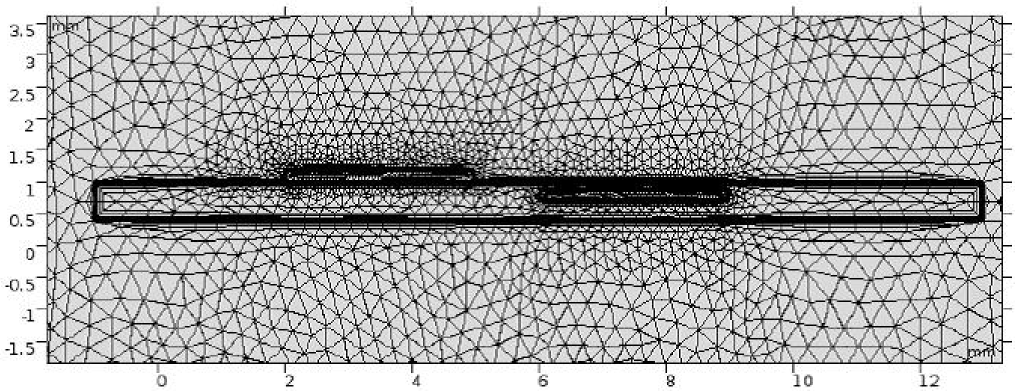

Figure 2: Mesh and its density at the sharp edge.

derived from non-elastic collisions calculated by the following equation:

$$R_e = S_{en} + \frac{Q + Q_{gen}}{q} \tag{4}$$

S_{en} is power dissipation, Q_{gen} is the thermal source and q is electron charge. D_e is electron diffusion coefficient, μ_e represents energy mobility, and D_ε is energy distribution coefficient. The relation between these parameters shows in Eq. (5):

$$\begin{aligned} D_\varepsilon &= \mu_\varepsilon T \\ D_e &= \mu_e T_e \\ \mu_\varepsilon &= \frac{5}{3}\mu_e \end{aligned} \tag{5}$$

We used the Townsend coefficients of the electron source that is calculated by the following equation:

$$R_e = \sum_{j=1}^{M} x_j a_j N_n |\Gamma_e| \tag{6}$$

in which M is the number of reactions, x_j is the molar fraction of the target species for the j reaction, a_j define the Townsend coefficient for the reaction j, and N_n is the total number of neutral particles. Considering the number p of non-elastic electron collisions, we will have:

$$R_\varepsilon = \sum_{j=1}^{p} x_j a_j N_n |\Gamma_e| \Delta\varepsilon_j \tag{7}$$

in which, $\Delta\varepsilon_j$ is the energy dissipation of j reaction. For non-electron induced species, the below equation is used for mass fraction calculation:

$$\rho\frac{\partial w_k}{\partial t} + \rho(\vec{u}.\nabla)w_k = \nabla.\vec{j}_k + R_k \tag{8}$$

in which, w_k is the ionic density, j_k is the energy flux of the ions. The electrostatic field is obtained by the following equation:

$$\nabla.(\varepsilon_0\varepsilon_r E) = \rho \tag{9}$$

where ε_0 is the permittivity of vacuum, and ε_r is a relative dielectric constant.

2.2 Boundary condition

With respect to the boundary conditions for the electron flux and energy flux, the following relations is obtained:

$$-\hat{n}.\vec{\Gamma}_e = (\frac{1}{2}\upsilon_{eth} n_e) - \sum_p \gamma_p(\vec{\Gamma}_p.\hat{n}) \tag{10}$$

$$-\hat{n}.\vec{\Gamma}_\varepsilon = (\frac{5}{6}\upsilon_{eth} n_e) - \sum_p \varepsilon_p\gamma_p(\vec{\Gamma}_p.\hat{n}) \tag{11}$$

The right-hand side of Eq. (10) shows the electron induced by the secondary electron and γ is the secondary electron coefficient. On the surface of electrodes, ions and excited species are neutralized by the surface reaction. Surface interactions on the electrode are indicated by the β_j coefficient, which indicates the probability of the function of the j species. Flux matching for each heavy species is defined as follows:

$$n.j_k = M_k R_{surf,k} + M_k c_k \mu_{m,k^z k}(n.E)[(z_k.n.E) > 0] \tag{12}$$

in which, j_k and $R_{surf,k}$ indicate the diffusive flux vector and the surface reaction rate expression for species k. M_k is mass fraction and c_p is particle mass density.

3 Results and discussion

In this study, the evolution of plasma characteristics by grounded electrode displacement are investigated. The transverse distance to the dielectric edge is 0.2 mm and the longitudinal distance from the electrode are considered 0.8 mm, 0.9 mm and 1 mm. Neumann is the chosen boundary conditions for free space and Dirichlet conditions for electrode surface (Fig. 1). Figure 3 shows the electrical potential in the presence of plasma at different distances of the electrodes. The power electrode voltage is 1000 V (DC) and the grounded electrode is at zero potential.

Figures 4 and 5 show the effect of grounded electrode displacement on electron and ion density at 10 ns. Increasing electrode distance, decrease the number of electron and ion density on the right side of the power electrode. The discharge starts at the right side of the power electrode

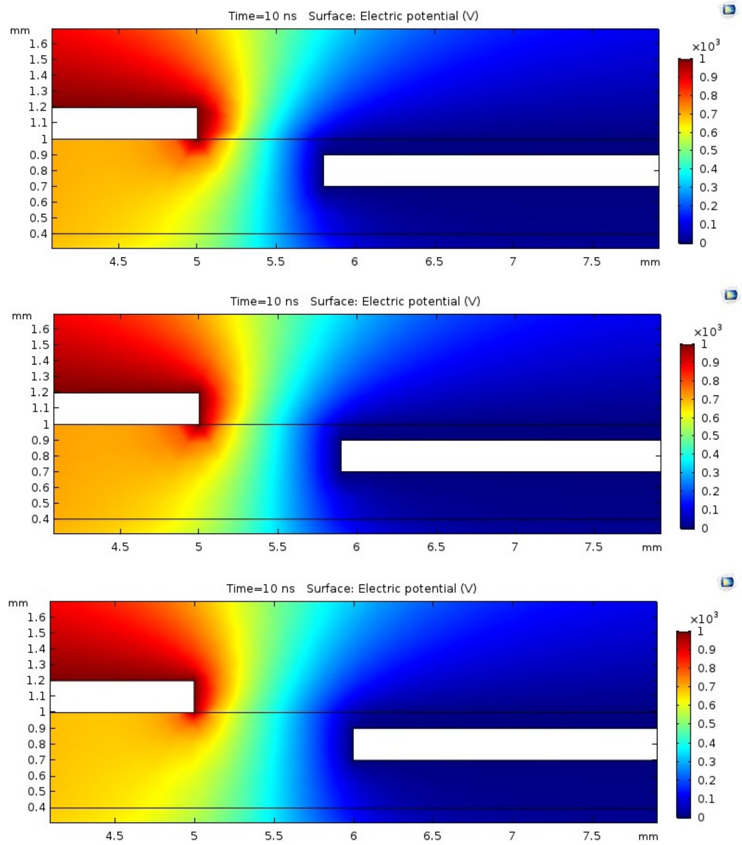

Figure 3: Electric potential distribution on the cross-section of the actuator for different distances of the electrodes (a) 0.8 mm (b) 0.9 mm (c) 1 mm.

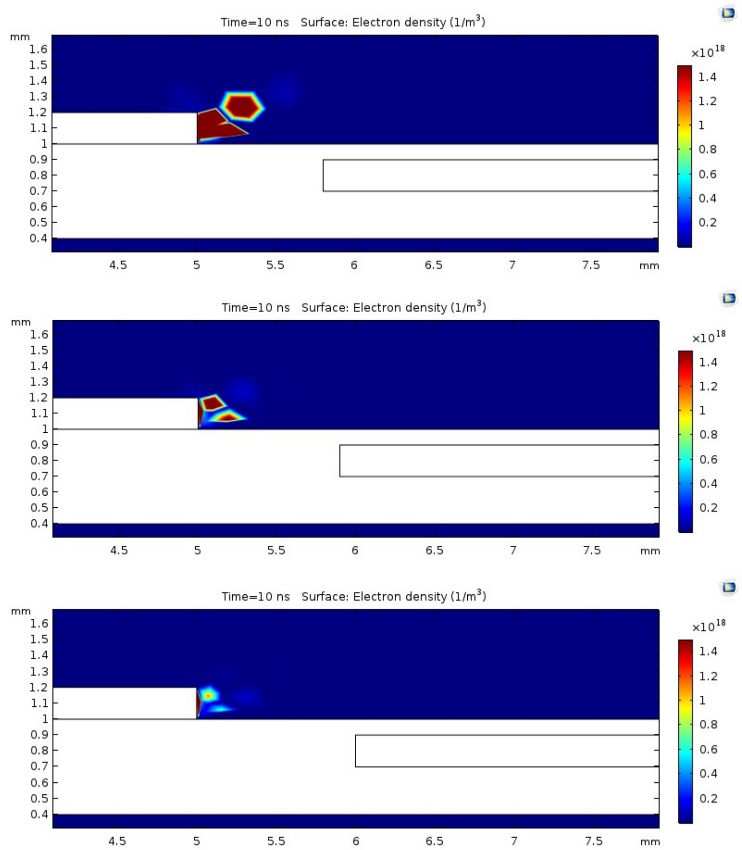

Figure 4: The electron density at 1 kV DC voltage over 10 ns for (a) 0.8 mm (b) 0.9 mm (c) 1 mm distances.

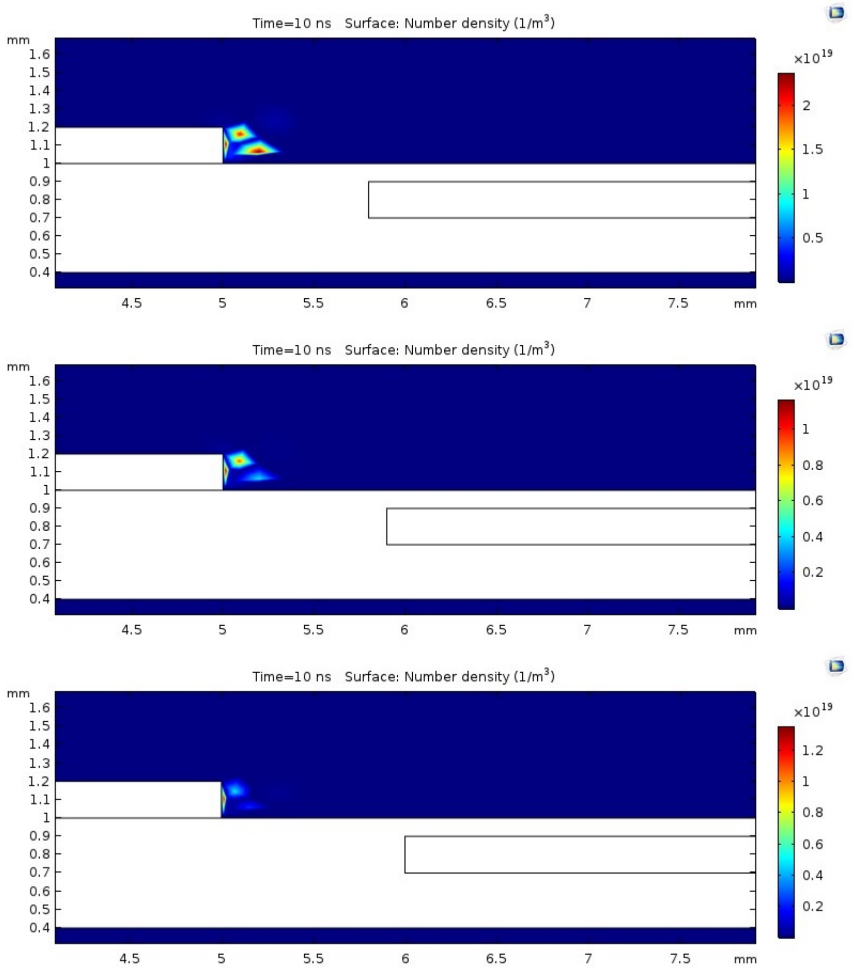

Figure 5: The ion density at 1 kV DC voltage over 10 ns for (a) 0.8 mm (b) 0.9 mm (c) 1 mm.

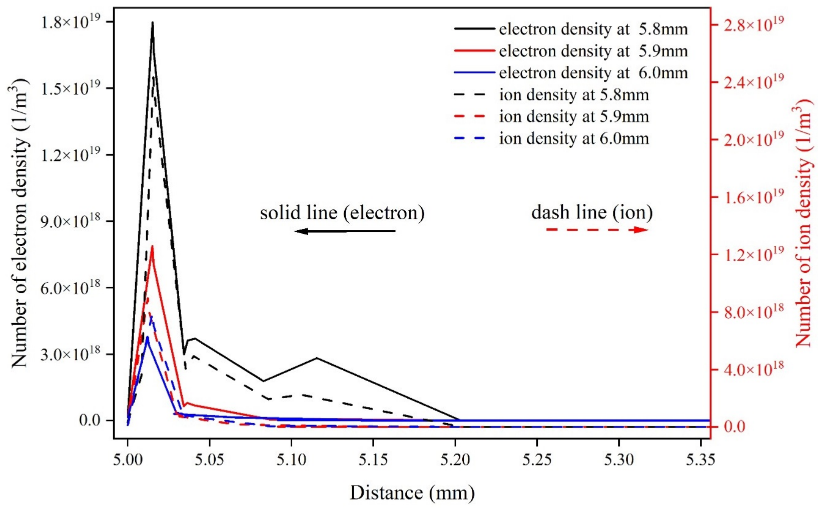

Figure 6: Electron and ion densities on the virtual line.

and propagates to the wall over time. The maximum electron density in the edge of the power electrode is 1.4×10^{18} m^{-3}.

The process of ion density changes in respect to distance from the electrode in this structure is more significant with the displacement of electrodes. The maximum electron density in the edge of power electrode is 2×10^{19} m^{-3}.

For more investigations about the electron and ion density changes due to the displacement of the grounded electrode. The electron and ion densities are shown on the upper side of the wall (Fig. 6). Figure 6 shows the ion

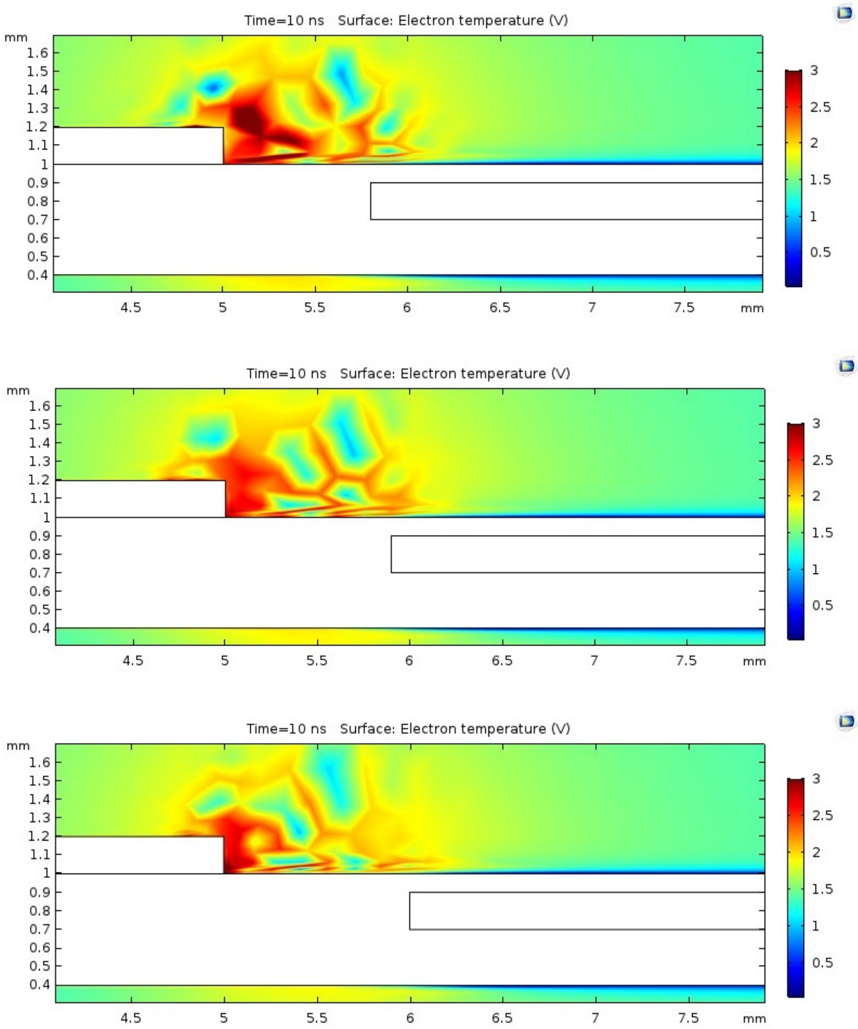

Figure 7: Electron temperature distribution at the discharge zone at 10 ns for (a) 0.8 mm (b) 0.9 mm (c) 1 mm distances.

and electron density changes on a virtual line from points $(x = 5, y = 1.1)$ to $(x = 9$ and $y = 1.1)$ for different displacements of electrodes. Variation in density is more significant for distances of 0.8 mm to 0.9 mm.

Figure 7 shows the electron temperature distribution at 10 ns for different distances of the electrodes. The electron temperature near the power electrode is the maximum value and by moving away from it, temperature reaches its minimum value (1 eV). The increase in the distance between the electrodes also reduces the electron temperature in the discharge zone.

One of the effective parameters in creating body force is the electric field. Increasing the electric field apart from the direction is the main factor in increasing the body force. In Fig. 8, the density of the field lines and the field size in the space between the two electrodes and above the dielectric surface are shown.

The dielectric material plays an important role in the rate of species production. Dielectric materials are electrically insulating materials that do not conduct electricity easily. When a plasma comes into contact with a dielectric material, several phenomena can occur that affect the behavior of the plasma and the production of species (Fridman and Kennedy, 2016; Lieberman and Lichtenberg, 1994). We studied the effect of three different dielectric materials on plasma parameters. The horizontal distance between the two electrodes is considered to be 1 mm here, and the species densities at the moment of 10 nanoseconds are shown in Fig. 9. Since the magnitude of the positive and negative charge difference has a direct effect on the magnitude of the body force, this value has been calculated for different dielectrics as shown in Fig. 10. The highest charge difference obtained for mica dielectric and the lowest one for silica glass. Actually, dielectric materials can modify the electric field distribution within a plasma system. This altered electric field can affect the transport and motion of charged particles, influencing their trajectories and interactions. Consequently, the modified electric field can impact the rate of species production by influencing the collisions and reactions occurring within the plasma. Moreover, the presence of plasma can induce changes in the surface properties of a dielectric material, such as surface roughness, chemical composition, or the formation of surface layers. These modifications can have implications for the interaction between the plasma and the dielectric, altering the species production rates.

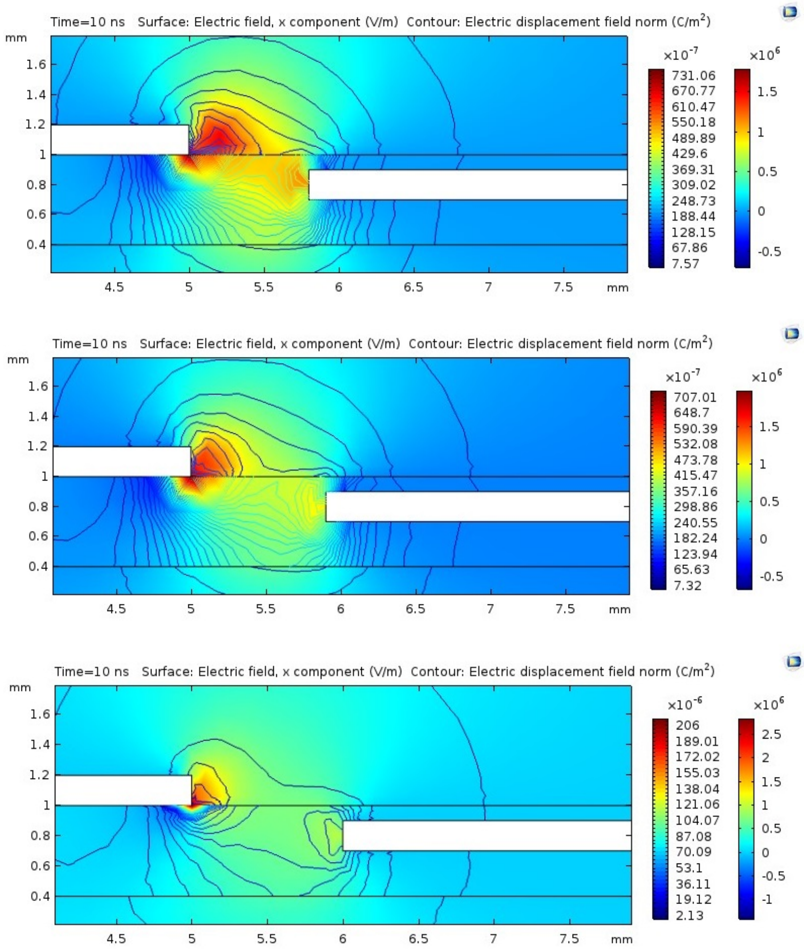

Figure 8: Density and magnitude of the electric field in plasma actuator for (a) 0.8 mm (b) 0.9 mm (c) 1 mm distances.

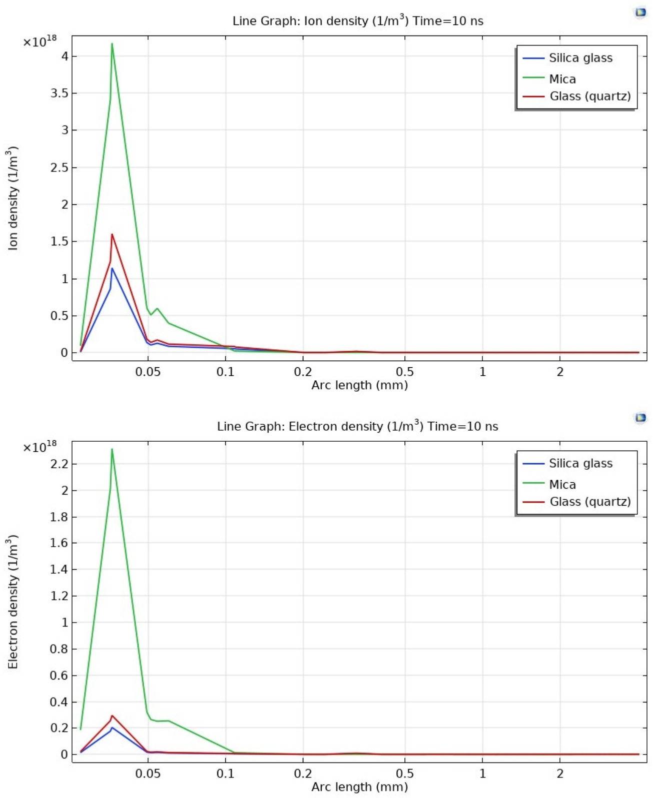

Figure 9: Ion density (up) and electron density (down) for different dielectric materials.

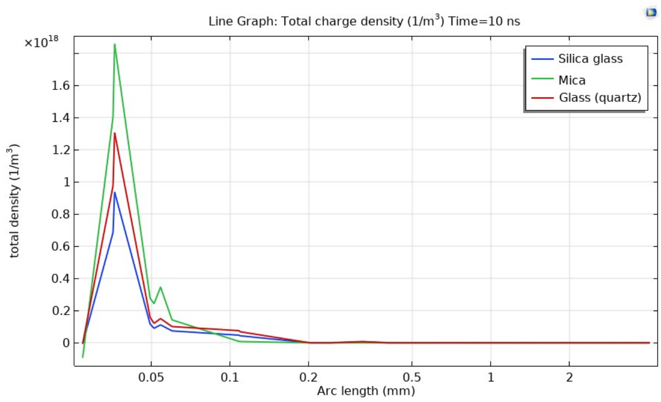

Figure 10: Net charge for different dielectric materials.

4 Conclusions

In this study, the electric discharge using Argon as working gas in plasma actuators has been studied in the two-dimensional structure. The species densities at different gap distances of the electrodes were studied. Seven possible reactions and two surface reactions on the dielectric are considered. The magnitude of the field and net electric charge in the discharge zone are the main factor of body force production. The results of the simulation of electrical discharge using Comsol Multiphysics show the significant effect of the grounded electrode distance on the body force. Longitudinal displacement of 0.1 mm (1.0 to 0.8 mm) distance from the power electrode has a significant effect on plasma parameters, including ion and electron densities and electrical parameters as electric field. Also, as a dielectric, Mica can create the largest charge difference compared to Quartz and Glass. The results of this simulation help us to determine the most optimal mode to create more body force.

Conflict of Interest

The authors declare no potential conflict of interest regarding the publication of this work.

References

Abdollahzadeh, M., Páscoa, J., and Oliveira, P. (2012). Numerical modeling of boundary layer control using dielectric barrier discharge. In *MEFTE IV Conferencia Nacional em Mecanica de Fluidos*.

Boeuf, J.-P., Lagmich, Y., Unfer, T., et al. (2007). Electrohydrodynamic force in dielectric barrier discharge plasma actuators. *Journal of Physics D: Applied Physics*, 40(3):652.

Da Ponte, G., Sardella, E., Fanelli, F., et al. (2012). Plasma Deposition of PEO-Like Coatings with Aerosol-Assisted Dielectric Barrier Discharges. *Plasma Processes and Polymers*, 9(11-12):1176–1183.

Fridman, A. and Kennedy, L. (2016). Nonequilibrium cold atmospheric pressure discharges. *Plasma Physics and Engineering*, pages 561–611.

Georghiou, G. E., Papadakis, A., Morrow, R., et al. (2005). Numerical modelling of atmospheric pressure gas discharges leading to plasma production. *Journal of Physics D: Applied Physics*, 38(20):R303.

Graves, D. B. (2012). The emerging role of reactive oxygen and nitrogen species in redox biology and some implications for plasma applications to medicine and biology. *Journal of Physics D: Applied Physics*, 45(26):263001.

Hati, S., Mandal, S., Vij, S., et al. (2012). Nonthermal plasma technology and its potential applications against foodborne microorganisms. *Journal of Food Processing and Preservation*, 36(6):518–524.

Jayaraman, B., Lian, Y., and Shyy, W. (2007). Low-Reynolds Number Flow Control Using Dielectric Barrier Discharge-Based Actuators. In *37^{th} AIAA Fluid Dynamics Conference and Exhibit*, page 3974.

Lieberman, M. A. and Lichtenberg, A. J. (1994). Principles of plasma discharges and materials processing. *MRS Bulletin*, 30(12):899–901.

Lukes, P., Dolezalova, E., Sisrova, I., et al. (2014). Aqueous-phase chemistry and bactericidal effects from an air discharge plasma in contact with water: evidence for the formation of peroxynitrite through a pseudo-second-order post-discharge reaction of H_2O_2 and HNO_2. *Plasma Sources Science and Technology*, 23(1):015019.

Mehrabifard, R., Mehdian, H., and Bakhshzadmahmoudi, M. (2017). Effect of non-thermal atmospheric pressure plasma on MDA-MB-231 breast cancer cells. *Pharmaceutical and Biomedical Research*, 3(3):12–16.

Mehrabifard, R., Mehdian, H., Hajisharifi, K., et al. (2020). Improving cold atmospheric pressure plasma efficacy on breast cancer cells control-ability and mortality using Vitamin C and static magnetic field. *Plasma Chemistry and Plasma Processing*, 40:511–526.

Shang, J. and Huang, P. (2010). Modeling of ac dielectric barrier discharge. *Journal of Applied Physics*, 107(11):113302.

Shang, J. and Huang, P. (2014). Surface plasma actuators modeling for flow control. *Progress in Aerospace Sciences*, 67:29–50.

Sohbatzadeh, F., Mehdipoor, M., and Mirzanejhad, S. (2019). Theoretical investigation of supersonic flow control by non-thermal DC discharge. *Shock Waves*, 29:415–426.

Soloviev, V. and Krivtsov, V. (2009). Surface barrier discharge modelling for aerodynamic applications. *Journal of Physics D: Applied Physics*, 42(12):125208.

Weltmann, K. D., Kindel, E., von Woedtke, T., et al. (2010). Atmospheric-pressure plasma sources: Prospective tools for plasma medicine. *Pure and Applied Chemistry*, 82(6):1223–1237.

Zimmermann, J. L., Dumler, K., Shimizu, T., et al. (2011). Effects of cold atmospheric plasmas on adenoviruses in solution. *Journal of Physics D: Applied Physics*, 44(50):505201.

To cite this article:

Mehrabifard, R. (2023). Two-dimensional simulation of argon dielectric barrier discharge (DBD) plasma actuator with COMSOL Multiphysics. *Radiation Physics and Engineering*, 4(4), 43-50.

DOI: 10.22034/rpe.2023.392080.1127

To link to this article: `https://doi.org/10.22034/rpe.2023.392080.1127`